ISSN 2278-3091
Volume 8, No.1.6, 2019
International Journal of Advanced Trends in Computer Science and Engineering
Available Online at http://www.warse.org/IJATCSE/static/pdf/file/ijatcse0681.62019.pdf
https://doi.org/10.30534/ijatcse/2019/0681.62019

Level Set Based Whole Heart Segmentation in Non-Contrast Enhanced CT Images

Siti Salasiah Mokri[1], M Iqbal Saripan[2], Abdul Jalil Nordin[3], Mohammad Hamiruce[4], Noraishikin Zulkarnain[5]

[1,5]Center for Integrated System Engineering and Advanced Technologies (INTEGRA), Faculty of Engineering and Built Environment, Universiti Kebangsaan Malaysia, 43600 UKM Bangi, Selangor, Malaysia, siti1950@ukm.edu.my

[2,4]Faculty of Engineering, Universiti Putra Malaysia, 43400 UPM Serdang, Selangor, Malaysia

[3]Faculty of Medicine and Health Sciences, Universiti Putra Malaysia, 43400 UPM Serdang, Selangor, Malaysia

ABSTRACT

Segmentation of the whole heat in CT images prior to lung radiotherapy is crucial to avoid undesirable radiation. In addition, heart segmentation is equally important in cardiovascular disease medical image analysis. However, heart segmentation in non-contrast enhanced CT image is a challenging problem due to the similarity of the grey level intensities of the heart with its surroundings. This paper aims to propose an automated heart segmentation method in non-contrast enhanced CT images. The method first identifies important slices during lung segmentation process to define an elliptical volume of interest (VOI) that approximately confines the heart region. Then 2D distance regularized (DRLSE) method is used to segment the heart slice by slice. The segmentation results are further improved by a refined elliptical VOI constructed from 3 different shapes of ellipses. Then 3 stages of DRLSE are used to obtain the final heart boundary. The segmentation results are validated based on Jaccard and Dice coefficients, false positive ratio (RFP) and false negative ratio (RFN) using 10 patient datasets where the average of Jaccard value of 0.86 and Dice value of 0.93 are obtained. Both values are more than 0.85 that indicates good heart segmentation in thoracic non-contrast enhanced CT image.

Key words : DRLSE, Heart Segmentation, Level Set, Non Contrast Enhanced CT, Thoracic CT

1. INTRODUCTION

The segmentation of the whole heart in medical images is important for two reasons [1]. First, in radiotherapy planning, the boundaries of the healthy organs need to be identified so that they are spared and not affected by the radiation during the radiotherapy treatment. Thus, in case of lung, liver, breast or lymphoma cancer radiotherapy plannings, the boundary of the whole heart should be determined prior to the treatment so that the effect of radiation can be avoided at this region. Undesirable radiotherapy exposure to the heart during treatment causes long term effect of cardiac toxicity to the patients that may aggravate their prognostic rate [2],[3]. On top of that, undesirable radiation could also damage the vascular endothelium and capillary vessels that may lead to coronary artery disease [2],[4]. Secondly, heart segmentation is also important for 3D visualization of coronary arteries to enable coronary artery calcium assessment in managing cardiovascular disease [5] and aortic valve disease [6]. The imaging of the heart is commonly carried out via computed tomography (CT), magnetic resonance, ultrasound and nuclear imaging. These images are used to determine the diagnosis, treatment planning as well as for interventional surgery [7] of cardiovascular patients.

Heart segmentation in non-contrast enhanced CT image is very challenging due to the difficulty in differentiating the heart with the surrounding tissues such as the liver and the diaphragm as these organs have almost similar grey level intensities. This is in opposite to the depiction of the heart in contrast enhanced CT image [8]-[12] where the boundary can be clearly recognized. Several methods for whole heart segmentation in CT images have been proposed ([1],[13]-[16]) that mostly utilized atlas or registration-based segmentation methods that are time consuming. In latest, Bui et al., [17] proposed random walk [18] mode segmentation method to segment the heart in contrast enhanced CT images where the heart and its substructures are clearly shown. This is different to the problem that is presented in this paper. This paper proposes an automatic heart segmentation method in non-contrast enhanced CT images [19] in which a 3D ellipsoidal volume of interest (VOI) is used to mask the heart while distance regularized level set (DRLSE) segmentation method is used to refine the segmentation results.

2. RESEARCH METHOD

The heart segmentation in non-contrast enhanced CT is carried out following the lung segmentation process described in [20]. The heart segmentation is initialized by identifying

the last slice at the upper thoracic region that contains the definite airway voxel denoted as S_{index} during the lung segmentation procedure. To determine the heart centroid at this slice, a convex hull image of the lungs is generated and is masked with the distance transform image of the lungs. The centroid is the point of maximum intensity of this image. Then a 2D Distance Regularized Level Set segmentation (DRLSE) [21], [22], [23] is implemented starting at this point to segment the heart region. The edge stopping function (1) is defined, in which $\nabla I(x, y)$ is the gradient of the image $I(x, y)$ that is scaled to [800, 1200] while G_σ is the Gaussian kernel.

$$g(x, y) = \frac{1}{1 + |\nabla(G_\sigma * I(x, y))|^2} \quad (1)$$

Table 1 displays the parameters used in the level set process. Once the heart region is obtained, it is fitted with an ellipse. Figure 1 shows an example of 2D DRLSE heart segmentation result over the gradient image and an ellipse that fits the heart region.

Table 1: DRLSE parameters for heart segmentation at S_{index}

Parameters	Value
Weight of the weighted length term, λ	3
Weight of the area weighted term, α	-20
Width of the Dirac Delta function, ϵ	1.5
Weight of the distance regularised term, μ	0.2
Number of iterations	200
Time step, Δ_t	1

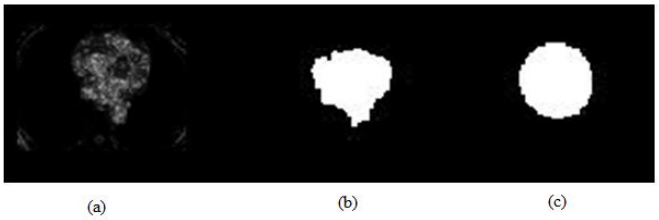

Figure 1: Fitting an ellipse on the segmented heart at S_{index} (a) edge function image (b) gross segmented heart after DRLSE (c) fitting a 2D ellipse on the gross segmented heart

The coronal plane that cuts the centroid of the fitted ellipse is then determined (Figure 2) to estimate the initial and the final slices of the heart, $S_{initial}$ and the S_{final} respectively. Taking the lungs as seen in the coronal plane, the convex hull image is created and is masked with the lungs to generate the distance transform image (Figure 2). The local maximum point of this image is obtained and the corresponding axial slice S_{center} is defined. Thus, $S_{initial}$ is estimated as:

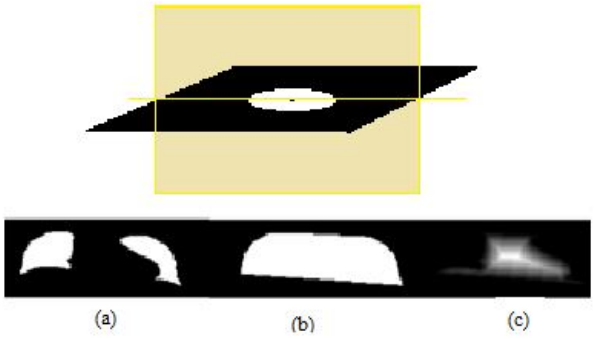

$$S_{initial} = S_{bifur} + round\left(\frac{1}{3} \times (S_{center} - S_{bifur})\right) \quad (2)$$

Figure 2: (Top) The axial and coronal planes that cross the centroid at S_{index} are determined. (Bottom) At the coronal plane (a) Lung mask (b) convex hull image (c) distance transform image

S_{final} is the last slice in which a vertical line emanated from the centroid cuts the convex hull image (Figure 3). S_{bifur} is the slice where the trachea bifurcates that is discovered during the lung segmentation process. The slice where the liver voxel appears, termed S_{liver} is also found by analysing the right lung volume from S_{index} to S_{final}. If the volume is reduced by 15% or more, S_{liver} is thus detected. At the S_{center}, 2D DRLSE is performed to obtain the heart region using the similar parameters as in Table 1. Then a 2D ellipse is fitted with a dilation of 5 pixels. A 3D ellipse is formed based on the 2D ellipse's centroid, the major radius and the minor radius while the height is (S_{final} - S_{middle})/2 with a margin of 5 slices. Two different rotation modes (5^0 about the *x* axis (coronal view) and 12.5^0 about the *y* axis (sagittal view)) are also implemented on the 3D ellipse to generate two other 3D ellipses. Figure 3 shows the definition of these important slices.

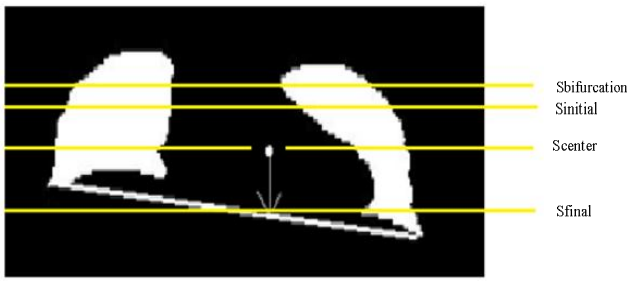

Figure 3: Determination of important slice indexes at the coronal plane

Bounded by the union of these three 3D ellipses, the 3D heart is estimated using 3 stages of 2D DRLSE slice by slice segmentation. The first stage is from S_{centre} to $S_{initial}$ where the zero level set for the current slice is the eroded heart region of the previous slice. The second stage is from S_{centre} +1 to S_{liver}

where the zero level set is a small circle at the centre point. In these two stages, the level set segmentation is in accordance to (1). The last stage is from S_{liver} +1 to S_{final} . At this stage, the DRLSE segmentation is based on (3) where $g_{1(x,y)}$ is an edge image of the scaled [950, 1200] CT (the range is chosen to highlight the soft tissue). The edge image is used in purpose of cautiously performed the segmentation as the heart intensity is comparably similar to the liver. $g_{1(x,y)}$ is then scaled to [0,255]. Then the inverse of g_1 is obtained as follows:

$$g^{\bullet}1 = \exp\left(-\frac{g_1(x,y)}{15}\right) \quad (3)$$

$g^{\bullet}_1$ is thresholded at 0.7 so that any pixel that is <=0.7 is kept. The segmentation is done on the $g^{\bullet}_1$ bounded by the obtained heart of the previous slice as in Figure 4.

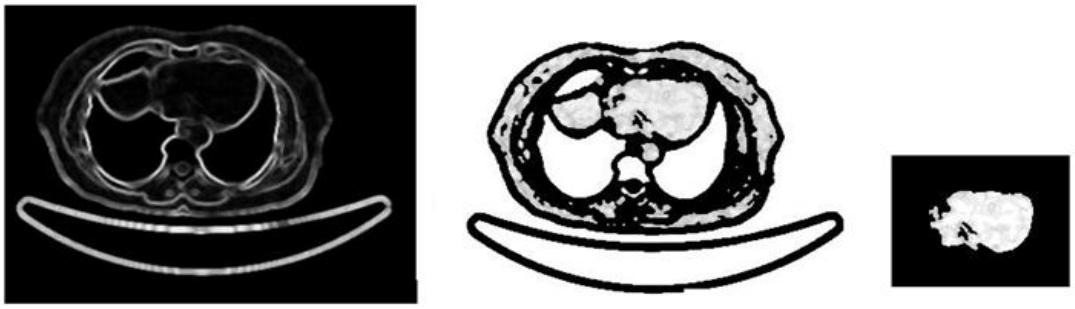

(a) (b) (c)

Figure 4: Derivation of edge function in the DRLSE third stage (a) Enhanced edge image (b) thresholded inversed edge image (c) image of (b) masked with bounded ellipse

Ultimately, the 3D gross estimation of the heart is obtained and fitted with a 3D ellipse. Six parameters are then extracted from the 3D ellipse , namely the minor long axis *a*; the major long axis *b*; the vertical radius *c*; the orientation angle of the segmented heart at axial (*x*-*y*) plane θ_1, the orientation angle of the segmented heart at coronal (*z*-*y*) plane θ_2 and the orientation angle of the segmented heart at sagittal (*z*-*x*) plane θ_3 (Figure 5). A more refined 3D mask that satisfactorily covers the heart region is then constructed based on a standard 3D ellipse of *a*, *b* and *c* setting followed with the rotation of θ_1, θ_2 and θ_3. The refined mask is considered as an ideal mask to further refine the heart segmentation. Finally, bounded by the ideal 3D mask, the three stages of DRLSE segmentation is once again carried out to obtain a more accurate 3D heart.

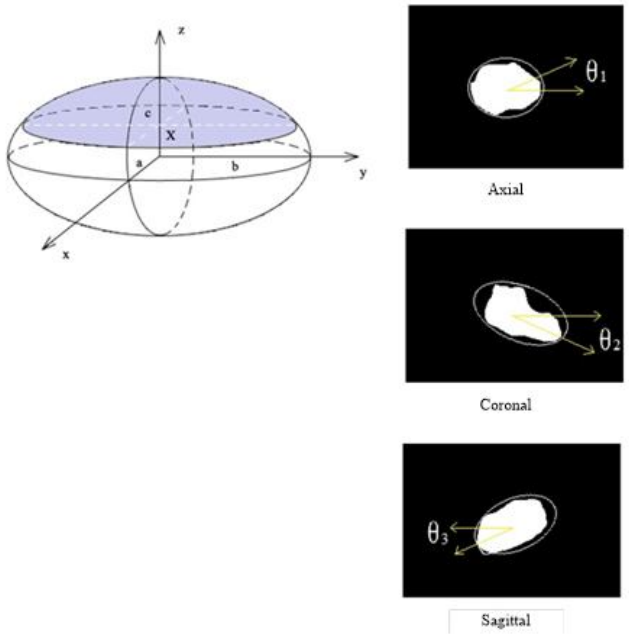

Figure 5: Graphical interpretation of the parameters to construct the ideal 3D ellipse

Non contrast enhanced CT images of 10 patients were acquired from the hybrid PET/CT machine of Biograph 6 (Siemens Medical Solutions Incorporated). The machine is available at the UPM Nuclear Diagnostic Imaging Centre (PPDN-UPM), Universiti Putra Malaysia, Malaysia. Table 2 shows the information of the datasets.

For quantitative evaluation, the segmented heart region using the proposed algorithm for each dataset was benchmarked against the manual segmentation by the expert attached to the PPDN-UPM Center. Four volume overlap parameters were used, Jaccard coefficient (Jaccard), Dice coefficient (Dice), false positive ratio (RFP) and false negative ratio (RFN) following to the ([24]-[26]). Considering *A* is the heart region resulting from the algorithm and *M* is the manual segmentation, each measure is defined as

$$Jaccard = \frac{A \cap M}{A \cup M} \quad (4)$$

$$Dice = \frac{2(A \cap M)}{(A \cap M) + (A \cup M)} \quad (5)$$

$$RFP = \frac{|A| - |A \cap M|}{|M|} \quad (6)$$

$$RFN = \frac{|M| - |A \cap M|}{|M|} \quad (7)$$

Table 2: Clinical non contrast CT image information

Descriptions	CT
Image size	512 x 512
Slice thickness	5mm
Pixel size	1.3672 mm
Bit depth	16

The Dice and Jaccard coefficients measure the spatial overlap between the automatic (*A*) and manual (*M*) segmentation results ranging from 0 (no overlap) and 1 (perfect overlap). RFP calculates the percentage of *A* voxels that are falsely included in the final segmentation according to *M* volume while RFN computes the percentage of missing *A* voxels that should be included in the final segmentation based on *M* volume. Both small RFP and RFN values, which are ideally 0, indicate good segmentation results.

3. RESULTS AND ANALYSIS

Visually, the segmented hearts in the tested datasets are satisfactory. The following Figure 6 – Figure 9 show the segmented heart for some of the patient datasets. As can be seen, in those figures, the heart regions have been well segmented for each patient as seen from the axial, sagittal and coronal views. Case of over segmentation can be seen at slices close to the diaphragm region due to ambiguous intensity difference between the heart and the diaphragm. Figure 10 shows the Jaccard, the Dice, the RFP and the RFN values for each heart segmentation result in which the *y* axis defines the obtained Jaccard, Dice, RFP and FRN values in the range of 0-1. Overall, the Jaccard and the Dice values are more than 0.75 and 0.85 respectively for the entire datasets. This achievement indicates that the algorithm performs satisfactorily. Segmentation result of the patient 3 dataset shows the best performance in terms of the highest Jaccard and Dice values while the RFP is almost zero. Table 3 tabulates the mean, the standard deviation, the maximum and the minimum values of each measures. Both Jaccard and Dice coefficient mean values exceed 0.8 (more than 0.85) which shows good segmentation results. The mean RFN is 7.33% (under segmentation) while the mean RFP is 6.05% (over segmentation). The mean Dice coefficient of more than 0.8 as achieved by the proposed method indicates that the segmentation is satisfactory based on Zijdenbos et al., [27] that defines good criteria for Dice similarity coefficient.

Table 3: Max, Min, Mean and Std of segmentation indexes for CT heart

Parameters	Max	Min	Mean	Std
Jaccard	0.9329	0.7705	0.8585	0.0442
Dice	0.9755	0.8804	0.9328	0.0417
RFP	0.1901	0.0019	0.0605	0.0531
RFN	0.1587	0.0280	0.0733	0.0307

Figure 6: Segmented CT heart for Patient 5

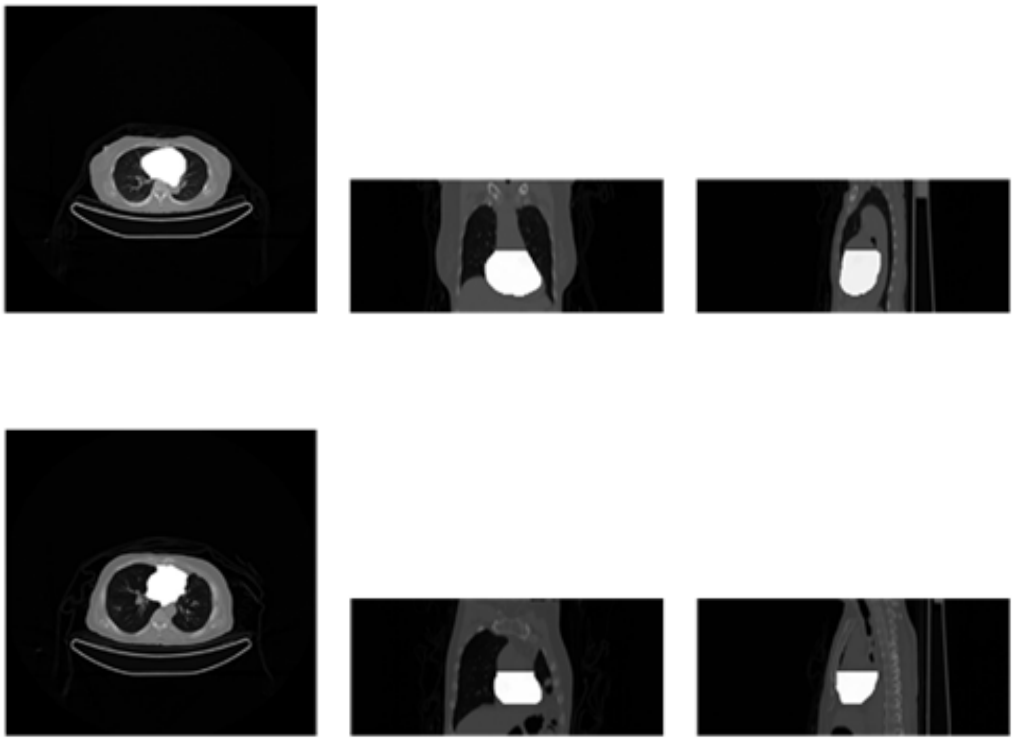

Figure 7: Segmented CT heart for Patient 6

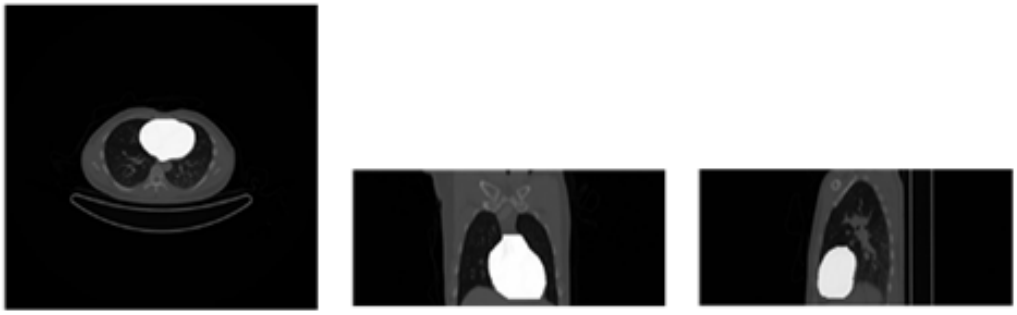

Figure 8: Segmented CT heart for Patient 7

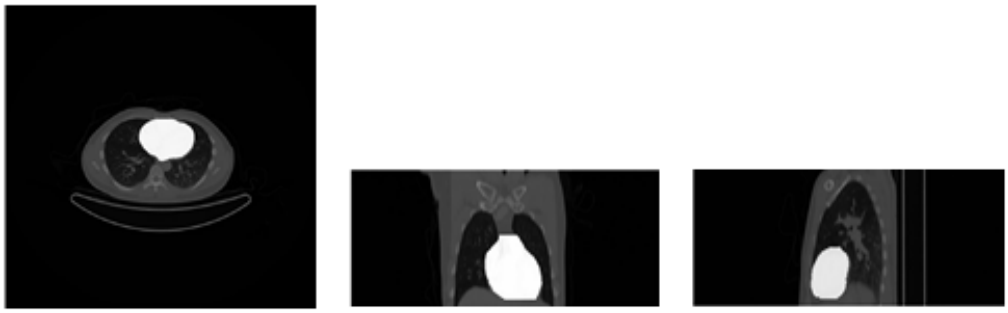

Figure 9: Segmented CT heart for Patient 9

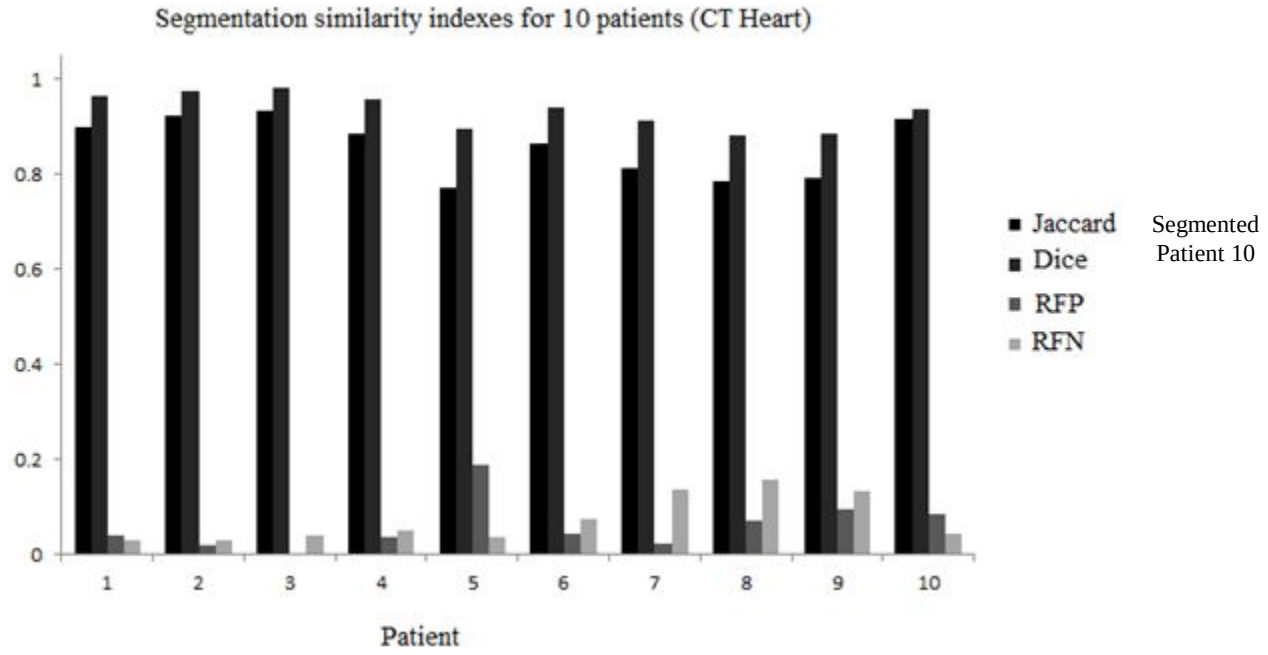

Figure 10: Segmented CT heart for Patient 10

Figure 11: Segmentation similarity indexes for CT heart

4. CONCLUSION

This paper proposes an automatic method to segment the heart in non-contrast enhanced CT images based on DRLSE method of three stages. Prior to the level set method, an important slice is initially found to start the segmentation process using the previously proposed lung segmentation method. Quantitatively, a good agreement between the proposed algorithm segmentation results with the expert delineation segmentation is obtained. In specific, the CT heart segmentation accuracy with respect to expert segmentation in terms of the average Jaccard and the Dice coefficients are 0.86 and 0.93 respectively which are more than 0.85. The achievement represents a good overlap between the proposed segmentation results with expert segmentation that implies good segmentation.

ACKNOWLEDGEMENT

The authors would like to acknowledge Kementerian Pendidikan Malaysia and Universiti Kebangsaan Malaysia through grant number FRGS/1/2019/TK04/UKM/02/5.

REFERENCES

1. Y. Zheng, F. Vega-Higuera, S.K. Zhou and D. Comaniciu. **Fast and automatic heart isolation in 3D CT volumes: optimal shape initialization,** *in 2010 international workshop on machine learning in medical imaging*, Springer, Berlin, 2010, pp. 84-91. https://doi.org/10.1007/978-3-642-15948-0_11
2. R. Zhou, Z. Liao, T. Pan, S.A. Milgrom, C. C. Pinnix, A. Shi and Q.N. Nguyen. **Cardiac Atlas Development and Validation for Automatic Segmentation of Cardiac Substructures**, *Radiotherapy and Oncology*, Vol. 122, no. 1, pp. 66-71, 2017. https://doi.org/10.1016/j.radonc.2016.11.016
3. Y. Luo, Y. Xu, Z. Liao, D. Gomez, J. Wang, W. Jiang, Z. Rongrong, W. Ryan, E.C. Laurence and J. Yang**. Automatic segmentation of cardiac substructures from noncontrast CT images: accurate enough for dosimetric analysis?**, *Acta Oncologica*, Vol. 58, no. 1, pp. 81-87, 2019.
4. R. Shahzad, D. Bos, R.P. Budde, K. Pellikaan, W.J. Niessen, A. van der Lugt, and T. van Walsum. **Automatic Segmentation and Quantification of the Cardiac Structures from Non-contrast-enhanced Cardiac CT Scans**, *Physics in Medicine & Biology*, Vol. 62, no. 9, pp. 3798, 2017. https://doi.org/10.1088/1361-6560/aa63cb
5. F.N. Rahaghi, G. Vegas-Sanchez-Ferrero, J.K. Minhas, C.E. Come, I. De La Bruere, J.M. Wells and P. Kohli. **Ventricular geometry from non-contrast non-ECG-gated CT scans: an imaging marker of cardiopulmonary disease in smokers**, *Academic radiology*, Vol. 24, no. 5, pp. 594-602, 2017. https://doi.org/10.1016/j.acra.2016.12.007
6. Y. Lu, Y. Sun, R. Liao and S. Ong. **A pre-operative CT and non-contrast-enhanced C-arm CT registration framework for trans-catheter aortic valve implantation**, *Computerized Medical Imaging and Graphics*, Vol. 38, no. 8, pp. 683-695, 2014.
7. Y. Zheng. **Model-Based 3D Cardiac Image Segmentation With Marginal Space Learning**,

Medical Image Recognition, Segmentation and Parsing, pp. 383-403, 2016.

8. K. Cai, R. Yang, H. Chen, L. Li, J. Zhou, S. Ou and F. Liu. **A framework combining window width-level adjustment and Gaussian filter-based multi-resolution for automatic whole heart segmentation**, *Neurocomputing*, Vol. 220, pp. 38-150, 2017. https://doi.org/10.1016/j.neucom.2016.03.106
9. R. S. Ahmed, J. Liu, Z. Fei and M. Zahid. **Automated segmentation of whole cardiac ct images based on deep learning**, *International Journal of Advanced Computer Science and Applications*, Vol. 9(4), 2018. https://doi.org/10.14569/IJACSA.2018.090464
10. J. Larrey-Ruiz, J. Morales-Sánchez, M.C. Bastida-Jumilla, R.M. Menchón-Lara, R. Verdú-Monedero and J.L. Sancho-Gómez. **Automatic image-based segmentation of the heart from CT scans**, *EURASIP Journal on Image and Video Processing*, Vol. 2014, no. 1, pp. 52, 2014.
11. F. Commandeur, M. Goeller, J. Betancur, S. Cadet, M. Doris, X. Chen and D. Dey. **Deep learning for quantification of epicardial and thoracic adipose tissue from non-contrast CT**, *IEEE transactions on medical imaging*, Vol. 37, no. 8, pp. 1835-1846, 2018. https://doi.org/10.1109/TMI.2018.2804799
12. O.C. Avila-Montes, U. Kurkure, R. Nakazato, D.S. Berman, D. Dey and I.A. Kakadiaris. **Segmentation of the thoracic aorta in noncontrast cardiac CT images**, *IEEE journal of biomedical and health informatics*, Vol. 17, no. 5, pp. 936-949, 2013. https://doi.org/10.1109/JBHI.2013.2269292
13. E.M. van Rikxoort, I. Isgum, M. Staring, S. Klein and B. van Ginneken. **Adaptive Local Multi-atlas Segmentation: Application to Heart Segmentation in Chest CT Scans**, *Medical Imaging, International Society for Optics and Photonics*, Vol. 6914, p. 691407, 2008. https://doi.org/10.1117/12.772301
14. A. Moreno, C.M. Takemura, O. Colliot, O. Camara and I. Bloch. **Using Anatomical Knowledge Expressed as Fuzzy Constraints to Segment the Heart in CT images**, *Pattern Recognition*, Vol. 41, no. 8, 2525-2540, 2008. https://doi.org/10.1016/j.patcog.2008.01.020
15. H. Zhong, Y. Zheng, G. Funka-Lea and F. Vega-Higuera, **Automatic Heart Isolation in 3D CT Images**, *International MICCAI Workshop on Medical Computer Vision*, 2012, pp. 165-180.
16. Y. Xie, M. Liang, D.F. Yankelevitz, C.I. Henschke and A.P. Reeves. **Automated segmentation of cardiac visceral fat in low-dose non-contrast chest CT images**, In *Medical Imaging 2015: Computer-Aided Diagnosis*, Vol. 9414, pp. 94140G, 2015. https://doi.org/10.1117/12.2081992
17. V. Bui, L.Y. Hsu, L.C. Chang and M.Y. Chen. **An Automatic Random Walk Based Method Computed Tomography images**, in *IEEE 15th International Symposium on Biomedical Imaging*, 2018, pp. 1352-1355.
18. S.J.A. Ibrahim and M. Thangamani. **Innovative Drug and Disease Prediction with Dimensionality Reduction and Intelligence Based Random Walk Method**, *International Journal of Advanced Trends in Computer Science and Engineering*, pp. 1668-1673, 2019. https://doi.org/10.30534/ijatcse/2019/93842019
19. S. A. Agnes and J. Anitha. **3D Lung Segmentation on CT images using Region Based Method**, *International Journal of Advanced Trends in Computer Science and Engineering*, pp. 1156-1161, 2019. https://doi.org/10.30534/ijatcse/2019/24842019
20. S.S. Mokri, M.I. Saripan, M.H. Marhaban and A.J. Nordin. **Lung Segmentation in CT for Thoracic PET-CT Registration Through Visual Study**, *IEEE-EMBS Conference on Biomedical Engineering and Sciences*, 2012, pp. 550–554.
21. C. Li, C. Xu, C. Gui and M.D Fox. **Distance Regularized Level Set Evolution and its Application to Image Segmentation**, *IEEE Transactions on Image Processing*, Vol. 19, no. 12, pp. 3243–54, 2010.
22. P. Yugander and G.R. Reddy. **Liver tumor segmentation in noisy CT images using distance regularized level set evolution based on fuzzy C-means clustering**, In *2017 2nd IEEE International Conference on Recent Trends in Electronics, Information & Communication Technology (RTEICT)*, 2017, pp. 1530-1534.
23. L. Jin-qing and L. Wei-Wei. **Adaptive medical image segmentation algorithm combined with DRLSE model**, *Procedia Engineering*, Vol. 15, pp. 2634-2638, 2011.
24. F. Yang and P.W. Grigsby. **Delineation of FDG-PET Tumors From Heterogeneous Background Using Spectral Clustering**, *European Journal of Radiology*, Vol. 81, no. 11, pp. 3535-3541, 2012.
25. N.S.M. Noor, N.M. Saad, A.R. Abdullah and N.M. Ali. **Automated segmentation and classification technique for brain stroke**, *International Journal of Electrical and Computer Engineering*, Vol. 9, no. 3, pp. 1832, 2019. https://doi.org/10.11591/ijece.v9i3.pp1832-1841
26. J. Muthuswamy and B. Kanmani. **Optimization Based Liver Contour Extraction of Abdominal CT Images**, *International Journal of Electrical and Computer Engineering*, Vol. 8, no. 6, pp. 5061, 2018.
27. A.P. Zijdenbos, B.M. Dawant, R.A. Margolin and A.C. Palmer. **Morphometric Analysis of White Matter Lesions in MR Images: Method and Validation**, *IEEE Transactions of Medical Imaging*, Vol. 13, pp. 716–724, 1994. https://doi.org/10.1109/42.363096